Full-scale tunnel experiments: blast wave and fireball evolution following hydrogen tank rupture.

S. Kudriakov[a,*], E. Studer[a], G. Bernard-Michel[a], D. Bouix[b], L. Domergue[c], D. Forero[a],

H. Gueguen[a], C. Ledier[a], P. Manicardi[b], M. Martin[b], F. Sauzedde[b]

[a] *DES, CEA, Université Paris-Saclay, Saclay, France,*

[b] *Univ Grenoble Alpes, CEA, LITEN, DEHT, LSP, F-38000 Grenoble, , France,*

[c] *DSSN, CEA, Université Paris-Saclay, Saclay, France*

Abstract

In the framework of the HyTunnel-CS European project sponsored by Clean Hydrogen Joint Undertaking (CH JU), a number of tests were conducted in a full-scale tunnel in France. These tests are devoted to safety of hydrogen-fuelled vehicles having a compressed gas storage. The goal of the study is to develop recommendations for Regulations, Codes and Standards (RCS) for inherently safer use of hydrogen vehicles in enclosed transportation systems. Two sets of tests have been performed, (a) five tests with compressed hydrogen tanks, (b) two tests with compressed helium tanks. The hydrogen gas pressure varied between 47 bar and 610 bar. The blast wave overpressures are recorded together with fireball characteristics. The obtained experimental data are compared to existing engineering correlations and it is confirmed that not only the mechanical energy of compressed gas but also a fraction of chemical energy contribute to the blast wave strength.

Keywords

Hydrogen safety, Tank rupture test, Blast wave decay, Fireball

HIGHLIGHTS

- Tank rupture tests are conducted in a full-scale tunnel.
- Compressed helium tanks as well as compressed hydrogen tanks are opened with detonation belts.
- Blast wave evolution with time and distance is analysed and compared to available correlations.
- Fireball evolution inside tunnel cross-section is filmed and analysed.

Nomenclature

Acronyms

AR	Aspect Ratio
CEA	Commissariat à l'énergie atomique et aux énergies alternatives
CGH2	Compressed Gaseous Hydrogen
CH JU	Clean Hydrogen Joint Undertaking
DB	Detonation Belt
ECF	Energy Concentration Factor
HFC	Hydrogen Fuel Cell
LH2	Liquid Hydrogen
PCB	PicoCoulomB
TNT	TriNitroToluene
TPRD	Thermally activated Pressure Relief Device

Greeks

π	PI constant
γ	Ratio of specific heats

Latins

AR	Aspect ratio (width-to-height ratio)
A_T	Tunnel cross-section area, m^2
a	Speed of sound, m/s
b	Co-volume constant, m^3/kg
D_T	Hydraulic diameter, m
E	Tank energy, J
E_{ch}	Chemical energy, J
E_{cin}	Kinetic energy, J
E_m	Mechanical energy, J
f	Friction factor
I	Impulse, $Pa \cdot s$ or $bar \cdot s$
$\bar{I}$	Non-dimensional implulse
L	Distance, m
$\bar{L}$	Non-dimensional distance
M	Gas molar mass
m	Compressed gas mass
$\bar{P}$	Non-dimensional pressure
p	Pressure, Pa or bar
$\bar{R}$	Universal gas constant, J/mol/K
r	Distance, m
T	Temperature, K

Subscripts

0	Related to atmospheric conditions
1	Related to compressed gas conditions
s	Related to shock-wave conditions

1. Introduction

Hydrogen Fuel Cell Electric Vehicles (HFC EVs) represent an alternative to replace current internal combustion engine vehicles. The use of these vehicles with storage of compressed gaseous hydrogen (CGH2) or liquid hydrogen (LH2) in confined spaces, such as tunnels, underground car parks, etc., creates new challenges to ensure the protection of people and property and to keep the risk at an acceptable level. Several studies have shown that confinement or congestion can lead to severe accidental consequences compared to accidents in an open atmosphere. It is therefore necessary to develop validated hazard and risk assessment tools for the behavior of hydrogen in tunnels. The HyTunnel-CS project sponsored by the CH JU pursues this objective.

One of the accidental scenarios involves a compressed hydrogen storage exposed to fire. Conventional high-pressure hydrogen tank is equipped with a thermally activated pressure relief device (TPRD) in order to prevent tank rupture during fire exposure. In case of failure of TPRD device, the high-pressure tank rupture can lead to harmful phenomena related, on one hand, to blast wave pressure effects, and, on the other hand, to thermal effects from a fireball. The situation can be aggravated inside a tunnel due to slower decay of the blast wave strength, compared to a tank rupture in open atmosphere. There is an obvious need for experimental data in order to validate the available correlations, which will constitute practical engineering tools.

Several pressurized tank rupture experiments have been conducted by Commissariat à l'énergie atomique et aux énergies alternatives (CEA) in June 2021 inside the Tunnel du Mortier located in the commune of Autrans in the Vercors, France. The tests can be divided into 2 categories: pressurized hydrogen gas tank rupture and pressurized helium tank rupture. The hydrogen gas pressure varied between 47 bar and 610 bar. The tanks were open with a detonation belt (DB) of RAZOR type. A fragment of each type of tank was ruptured with a DB alone in order to measure its contribution to the blast wave strength. The blast wave overpressures are recorded at different distances from the explosion and analyzed together with the behavior of large-scale fireballs.

The experiments on hydrogen tank rupture have been conducted previously only in open atmosphere [1] [2], and in all cases, a pressurized tank was installed over a fire. The TPRD devices were either not installed [1] or failed to be activated [2]. Similar experiments on hydrogen tank rupture inside tunnels have never been performed up to now. A number of experimental studies have been done *with solid explosives* positioned inside tunnels or steel pipes (for references see [3]). However, as it is analyzed in [4] and [5], a solid-explosive blast wave is different from the blast wave resulting from hydrogen pressurized tank rupture due to additional contribution of chemical energy.

From the phenomenological point of view, energy contained inside a high-pressure hydrogen tank can be split into mechanical energy of compressed gas and into chemical energy of

combustion when hydrogen is released into air. The value of chemical energy is at least one order of magnitude larger than the corresponding amount of mechanical energy. The open question is whether chemical energy contributes to the blast wave strength and, if yes, what is the contributing fraction of this energy? In order to answer this question, the explosion tests of helium-pressurized tanks having similar mechanical energy to the hydrogen-pressurized tanks were realized.

The paper is organized as follows. In Section 2, the geometry of the Tunnel, the tanks used for explosion tests, the pressure measurement devices as well as the test matrix are described. The test results are provided in Section 3, where the overpressure evolutions, maximum measured overpressure values are given for each test. Analysis of the experimental data in terms of the fraction of mechanical and chemical energy contained in a tank is presented as well. The fireball evolutions resulting from hydrogen tanks explosion are presented and analyzed in this Section. Conclusions follow in Section 4.

2. Tunnel geometry, Measurement Devices and Experimental Matrix

The Tunnel du Mortier is 507 m long disused straight road tunnel having horseshoe cross section shape (Figure 1). All experimental equipment, including the gas-filling platform and the measurement station, have been installed close to one of the entrances, further called Autrans entrance. Close to this entrance, the tunnel vault is concreted (Images 1 and 2 of Figure 1) while the major part of the rest of the tunnel is in rough rock (Images 3 and 4 of Figure 1). The concrete section is 133 m long, 7.5 m wide and 5.2 m high. The rocky area represents the largest part of the length with a width of 8.9 m and a height of 5.6 m. The tunnel slope is 3.6% and there is no mechanical ventilation. Finally, another concrete section is located at the other exit of the tunnel. The cross-section area in the rock part of the tunnel is approximately 41.3 m^2 while in the concrete part it is 33.0 m^2.

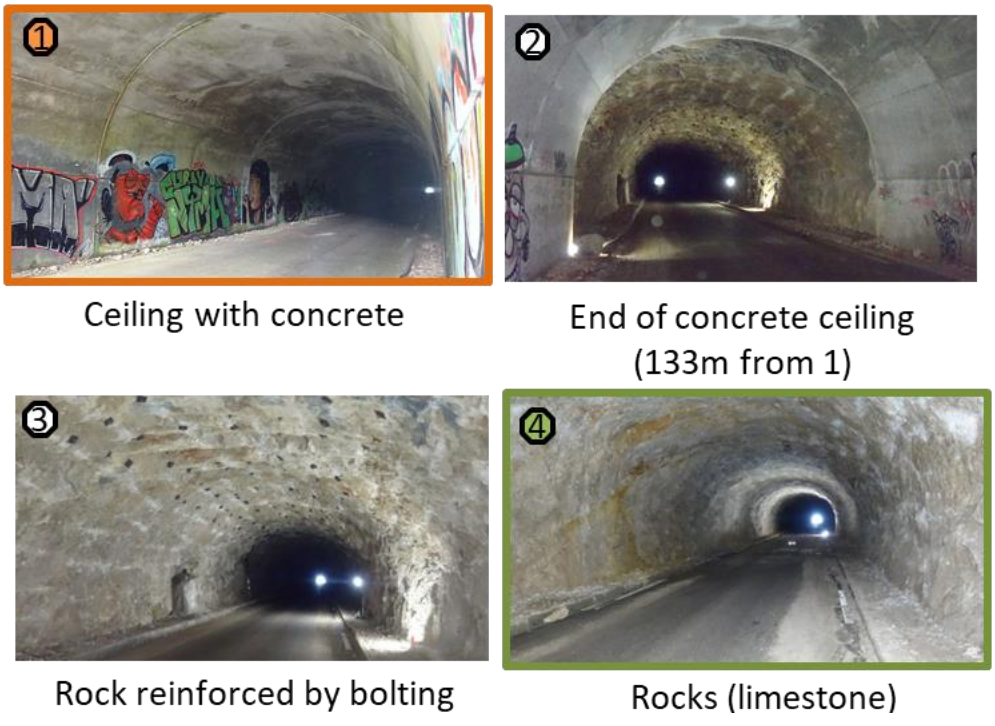

Figure 1: Tunnel geometry showing a concrete part (Images 1 and 2) as well as a rock part (Images 3 and 4).

All explosion tests were performed inside the tunnel at a distance of 228 m from the Autrans entrance. Two straw walls were installed at each end of the tunnel to limit natural convection and to quench the pressure waves.

In order to capture the pressure waves during the explosion tests, seven PCB blast wave pencils were arranged in the tunnel at distances of 30 m, 50 m, 80 m, 110 m, 140 m, 170 m and 200 m from the tank (Figure 2, left, Table 1). These sensors are mounted on tripods approximately 70 cm above the ground (Figure 2, right). We mention that the pressure transducer at 200 m did not function properly during the tests and all the measurements from this transducer, apart from one measurement, were disregarded. The blast wave pencil installed at 80 m from a tank is equipped with two pressure transducers, denoted P3A and P3B in Table 1. They are mounted 10 cm apart in order to monitor the velocity of the blast waves.

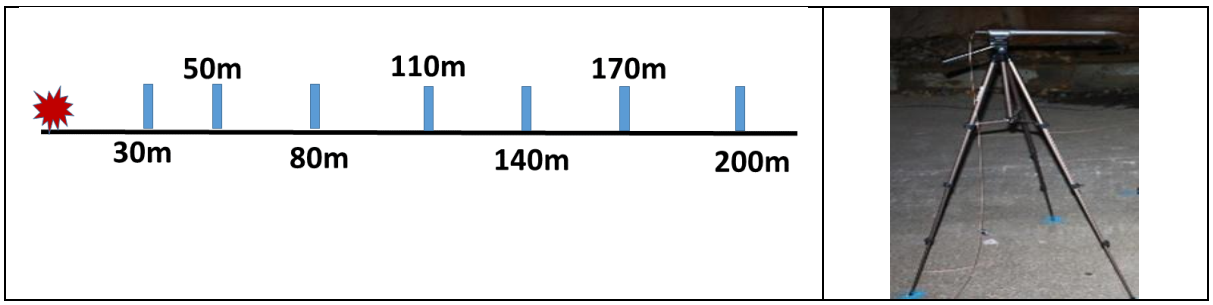

Figure 2 : Scheme of installation of blast wave pressure transducers (left) and photo of a PCB blast wave pencil.

Table 1 : Blast wave sensors positions

Sensor	X (mm)	Y (mm)	Z (mm)
P1A	0	30000	685
P2A	0	50000	685
P3A	0	80000	685
P3B	0	80100	685
P6A	0	110000	685
P7A	0	140000	685
P8A	0	170000	685
P5A	0	200000	685

In most of the experiments presented in the literature (see [1] [2] and references therein), the tank is set on fire and if there is no depressurization means (or they malfunction), the tank ends up exploding. In order to simplify the procedure and guarantee reproducibility, we have chosen to open the pressurized tank using a detonation belt of RAZOR type. This belt is located at the middle of the tank (Figure 3) and a small amount of explosive initiates its explosion. As far as possible, we tested the tanks with two different gases: helium or hydrogen. Systematically, for each tank, after the first explosion we kept a fragment and re-tested it with the detonating belt alone to measure its contribution. Type II and IV tanks were used for these tests with different inner volumes (Table 2, Figure 3); the “Tank Mass” corresponds to the mass of its solid structure only.

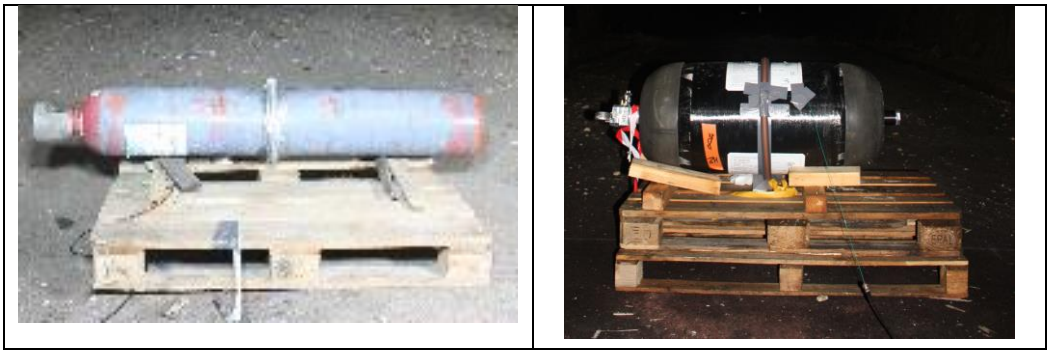

Figure 3 : Tanks used for explosion experiments: TYPE II (left) and TYPE IV (right). The detonation belt is attached to each of the tanks.

Table 2 : Specifications of Pressurized Tanks used in explosion tests

Tank name	Tank Volume (l)	Tank Mass (kg)	Tank length / ext.diameter (m)
TYPE II	50	60.5	1.45 / 0.3
TYPE IV	78	64.6	0.96 / 0.44

The Test Matrix is presented in Table 3. Two tests have been performed with empty tanks (Test 1 and 2), two tests with helium gas inside (Test 3 and Test 4), and four tests with hydrogen filled tanks (Tests 5-8). We mention that an additional test (Test 20) with hydrogen filled tank was conducted in 2020 during the preliminary experimental campaign (results can be found in [6]) and we shall integrate some of the results in this paper for completeness. The hydrogen gas pressure varied between 47 bar and 610 bar. The detonation belt charge is kept constant for each tank type, its energy is given in TNT equivalent units, i.e. 130 g for type II tank and 228 g for type IV tank (the Test 7 was performed with slightly lower charge, 221 g TNT). The outside air temperature was close to 15°C and atmospheric pressure – to 87 kPa for all explosion tests of the 2021 experimental campaign.

Table 3 : Test Matrix

Test N°	Tank	Gas	Pressure (bar)	Detonation belt charge (g, TNT)	Temperature, °C
1	TYPE II (frag.)			130	
2	TYPE IV (frag.)			228	
3	TYPE II	He	185	130	15
4	TYPE IV	He	650	228	15
5	TYPE IV	H2	90	228	15
6	TYPE II	H2	194	130	15
7	TYPE IV	H2	520	221	15
8	TYPE IV	H2	610	228	15
20	TYPE II	H2	47	130	10

3. Test results and analysis.

Blast wave propagation: experimental data

The sample rate for all pressure transducers was 200 kHz. A pressure signal contains a certain amount of noise, which is manifested itself by high frequency oscillations. These oscillations could be due to acoustic waves inside the metallic structures supporting the pressure transducers as well as the acoustic waves propagating inside the tunnel solid floor. The "useful" oscillation frequencies are those related to acoustic/shock waves propagating through the tunnel atmosphere. The speed of these waves (see Figure 14) was close to 350 m/s. We remind that the tunnel width and height in the zone near the explosion are 8.9 m and 5.6 m, respectively. This gives us time scales of 51 ms and 32 ms corresponding to the times necessary for the acoustic waves to travel back and forth either between lateral walls or between the ceiling and the floor of the tunnel. These would correspond to oscillating frequencies of 20 Hz and 31 Hz, respectively. The pressure transducers were located midway between lateral walls of the tunnel, which means that the related frequency recorded by the transducers is close to 40 Hz.

We performed a Fourier transform of the pressure signals and, as an example, the related magnitude spectrum is presented in the Figure 4 (right). One can see that the well-defined peak is present, corresponding to frequencies of around 40-50 Hz. Each pressure signal has been filtered using 4th order Butterworth low-pass filter with cut-off frequency of 100 Hz. The raw and filtered pressure signals recorded by transducer P1 are shown in Figure 4 (left). In what follows, we shall present only filtered signals for all tests.

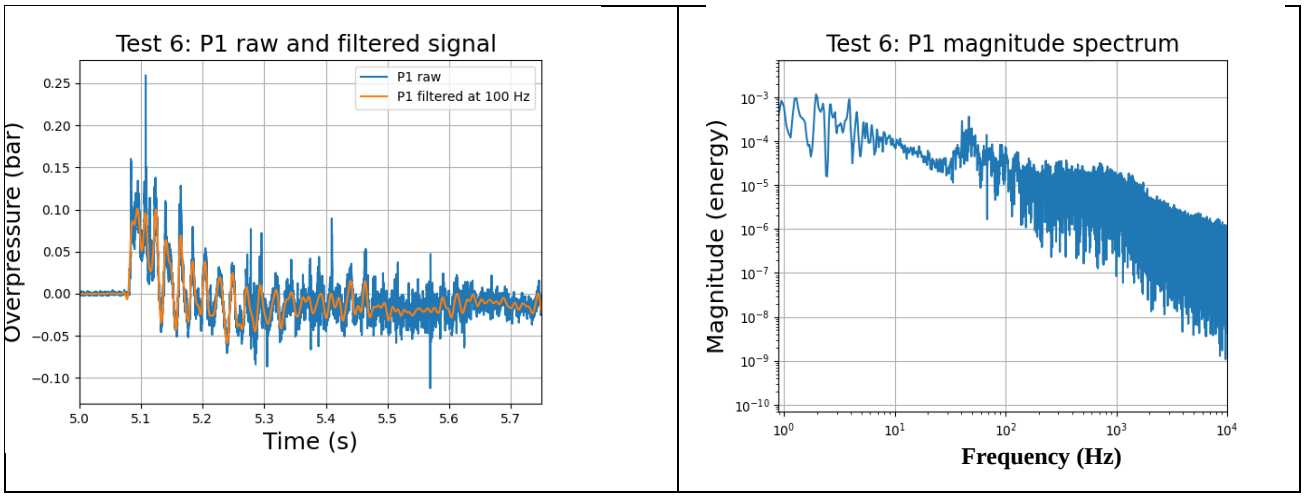

Figure 4 : ***Test 6****. Raw and filtered pressure signal at P1 (left, 30 m from explosion) and the magnitude spectrum of the pressure signal (right).*

Overpressure signals for Test 1 and Test 2 (Tanks fragment)

In Figure 5 and Figure 6 we present the pressure evolution with time at different distances for the Test 1 and the Test 2, respectively. Three observations can be made. *First*, we can separate the blast wave run-up distance on Zone 1, where pressure signals are dominated by blast wave reflections, and Zone 2, where the planar structure of the blast wave is observed, in the spirit of numerical observations reported in [5]. The transducers P1 (30 m), P2 (50 m) and P3 (80 m) are located in the Zone 1, while P6 (110 m), P7 (140 m) and P8 (170 m) - in the Zone 2. At a certain distance from the explosion, somewhere between 80 m and 100 m, the secondary waves coalesce with the leading front and the resulting blast wave propagates as a planar structure. *Second*, the pressure signal propagates with velocity close to 350 m/s which is slightly higher than the acoustic velocity, equal to 340 m/s (T = 15°C). *Third*, some non-physical oscillations

are observed on the signals corresponding to the transducers P6 (110 m), P7 (140 m) and P8 (170 m). After additional analysis, these oscillations have been attributed to the perturbations created by the blast wave on the instrumentation box. This box, containing the recording equipment, was located approximately at 70 m from the explosion for initial few tests and at 100 m from the explosion, for the rest of the tests.

The maximum overpressure levels measured at the ***first*** pressure peak are reported in Table 4. We can observe that the maximum pressure attenuation with distance is limited due to focalisation of the blast wave energy along the tunnel. We mention that at 87 m from the explosion, the cross section area of the tunnel diminishes from $41.3m^2$ down to $33m^2$. This could explain the maximum pressure increase measured by the transducers located after that distance. Overall, almost all the maximum overpressure levels are lower than 20 mbar, which is considered as the threshold for indirect effects with respect to human health [7].

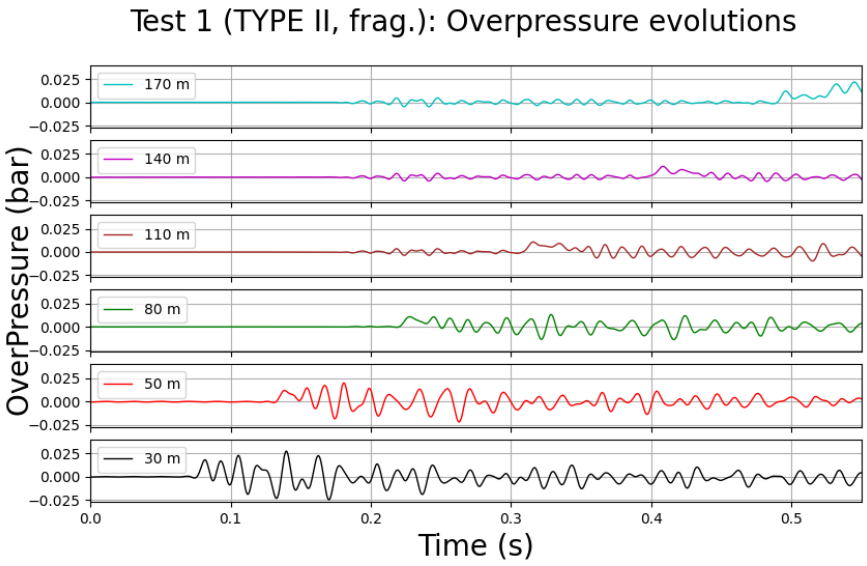

Figure 5: ***Test 1. Empty tank with DB of 130 g TNT****. Overpressure evolutions at different distances.*

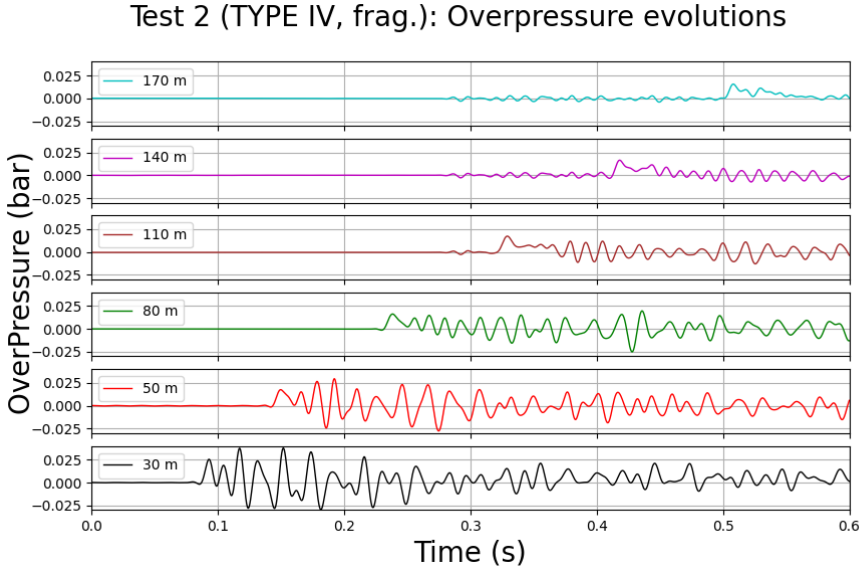

Figure 6: ***Test 2. Empty tank with DB of 228 g TNT****. Overpressure evolutions at different distances*

*Table 4 : **Tests 1-2 (fragments).** Maximum overpressures recorded at different distances*

Test	ΔP (mbar) @ 30 m	ΔP (mbar) @ 50 m	ΔP(mbar) @ 80 m	ΔP (mbar) @ 110 m	ΔP (mbar) @ 140 m	ΔP (mbar) @ 170 m
1	17.9	12.1	10.8	10.7	11.6	12.1
2	25.4	17.5	16.3	17.4	16.5	15.7

Overpressure signals for Test 3 and Test 4 (Tanks filled with Helium)

In Figure 7 and Figure 8 we present the pressure evolution with time at different distances for the Test 3 and the Test 4, respectively. These tests correspond to the pressurised helium tank rupture; thus only mechanical energy input into the overpressure evolution is considered. The observations made in the previous paragraph are valid here as well. The pressure oscillations, at distances 30 m and 50 m from explosion, are of relatively high amplitude and some of the pressure peaks at later times are higher than the first pressure peak. Those pressure peaks have to be considered with caution, as they could be the results of reflected pressure due to secondary waves propagation, and not the result of side-on pressure record. We deliberately cut the pressure signal P8 (170 m) (see Figure 8) due to the non-physical behaviour of the signal; the transducer fell down due to explosion.

The maximum pressure levels measured at the ***first*** pressure peak are reported in Table 5. We can observe, as before, that the maximum pressure attenuation with distance is limited due to focalisation of the blast wave energy along the tunnel. Overall, all the maximum overpressure levels are lower than 50 mbar, which is the threshold for irreversible effects with respect to human health (Test 3), and 140 mbar, representing the threshold for the first lethal effects (Test 4) [7].

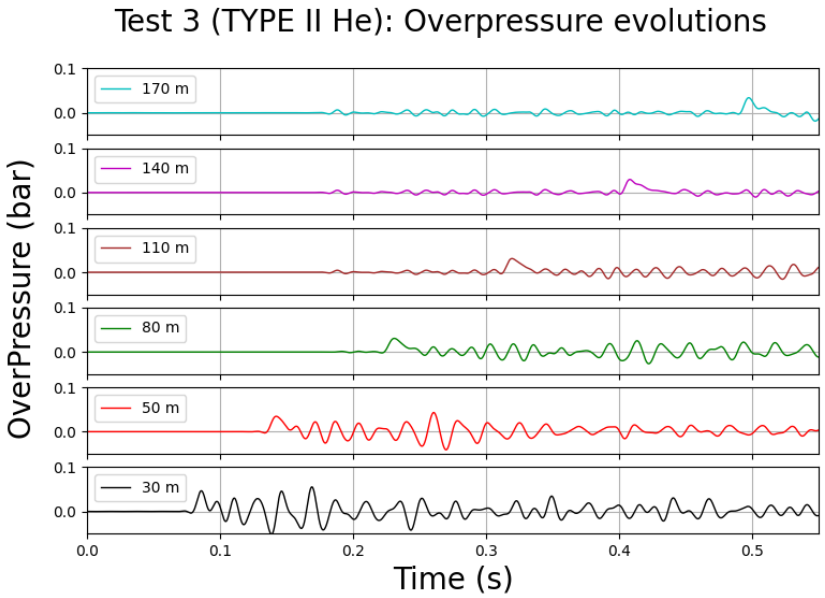

*Figure 7: **Test 3. He 185 bar, 50L Type II tank.** Overpressure evolutions at different distances*

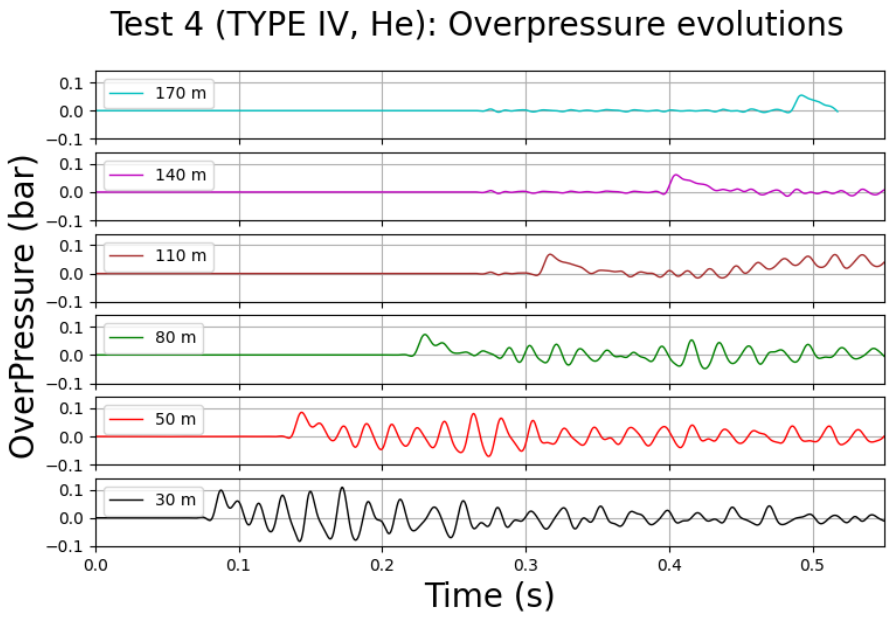

Figure 8: ***Test 4. He 650 bar, 78L Type IV tank.*** *Overpressure evolutions at different distances.*

Table 5 : ***Tests 3-4 (Helium tanks).*** *Maximum overpressures recorded at different distances*

Test	ΔP (mbar) @ 30 m	ΔP (mbar) @ 50 m	ΔP(mbar) @ 80 m	ΔP (mbar) @ 110 m	ΔP (mbar) @ 140 m	ΔP (mbar) @ 170 m
3	46.5	34.7	30.7	30.9	29.5	34.0
4	98.0	85.0	72.4	68.0	61.2	54.6

Overpressure signals for Test 5-8 (Tanks filled with Hydrogen)

In Figure 9 to Figure 12, we present the pressure evolution with time at different distances for the Tests 5 to 8, respectively. These tests correspond to the pressurised hydrogen tank rupture; thus, not only mechanical energy, but also chemical energy input into the overpressure evolution is considered. The observations made in the previous paragraph are valid here as well. As in the case with pressurized helium tanks, we deliberately cut some pressure signals (see Figure 9 to Figure 12) due to non-physical behaviour; the corresponding transducers fell down due to explosion. In all Figures we show the zoomed part of the pressure signals near the first pressure peak. In Figure 12 (bottom) we present the complete signal corresponding to the Test 8. We can see that the low frequency oscillations persist around zero value; they correspond to the acoustic waves travelling back and forth between two straw walls. The second pressure spike at approximately 1 second of the pressure signal at P7-140 m (red curve in Figure 12, bottom) corresponds to the reflection of the blast wave from the straw wall closest to the Autrans entrance.

Different behavior of the pressure peaks at close distances to the explosion point can be observed, in comparison to the previous tests. We can see that the first peak is not well defined; there are double or, sometimes, triple small peaks on the top of the main “global” peak. Moreover, the first small peak is not the highest one; very often, the second small peak has a higher value.

This behavior can be explained by recording of multiple pressure reflections or by initial liberation of chemical energy, or both. In the Figure 13 we present a sketch describing propagation of pressure waves due to explosion. A pressure transducer located at distance L from the explosion will record the first pressure peak at time t_L, corresponding to the shortest distance between the explosion and the transducer. Another pressure peak will be recorded when the blast wave, travelling upwards, hits the ceiling and is reflected towards the transducer via diagonal D at time t_{H+D}. Taking into account the averaged blast wave velocity of 350 m/s, we can readily compute the time difference for a particular distance L, $\Delta t = t_{H+D} - t_L$. This gives us a times scale: $\Delta t = 17\ ms$ and $\Delta t = 16.6\ ms$ for transducers located at 30 m and 50 m from explosion, respectively. The measured time difference between the consecutive small peaks is very close to these values.

In Table 6 we present the maximum overpressure values at different distances. By default, the values corresponding to the first peak are presented; in the brackets we present the values of the corresponding second pressure peaks, *if these values are higher than the corresponding values of the first peak.* From the results we can see that the maximum overpressure levels for the Tests 7 and 8 are higher than 200 mbar, the threshold for significant lethal effects with respect to human health [7].

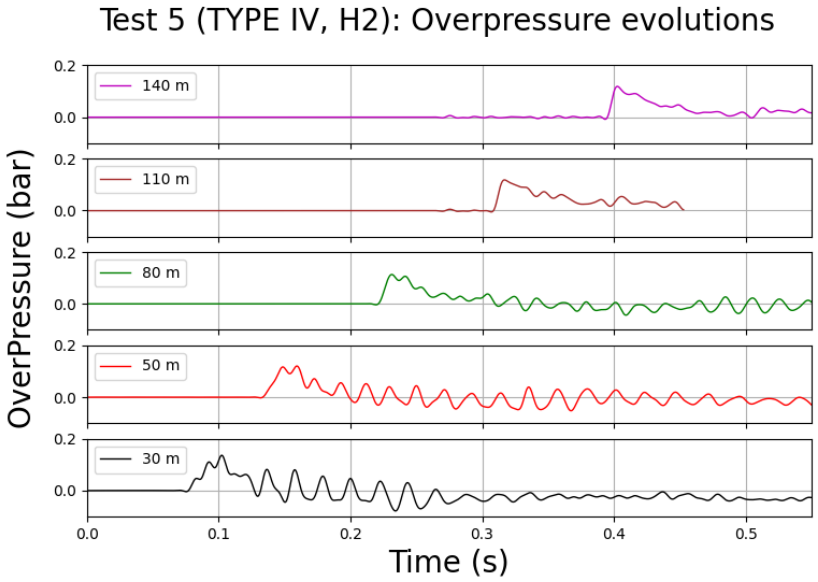

Figure 9: ***Test 5. H2 90 bar, 78L Type IV tank****. Overpressure evolutions at different distances*

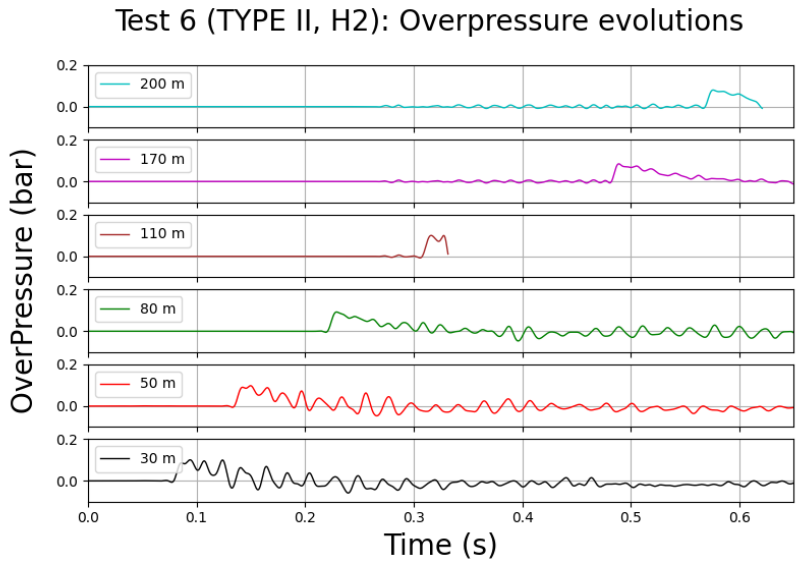

Figure 10: ***Test 6. H2 194 bar, 50L Type II tank****. Overpressure evolutions at different distances*

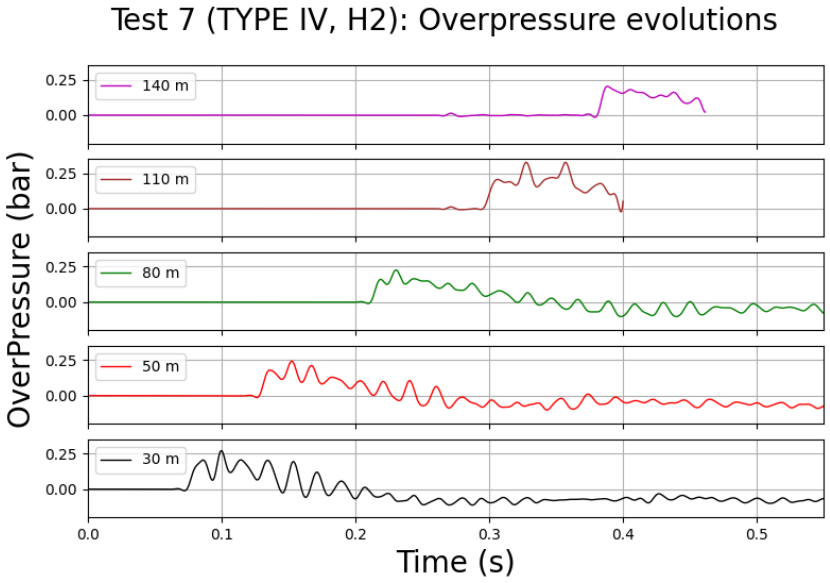

Figure 11: ***Test 7. H2 520 bar, 78L Type IV tank****. Overpressure evolutions at different distances*

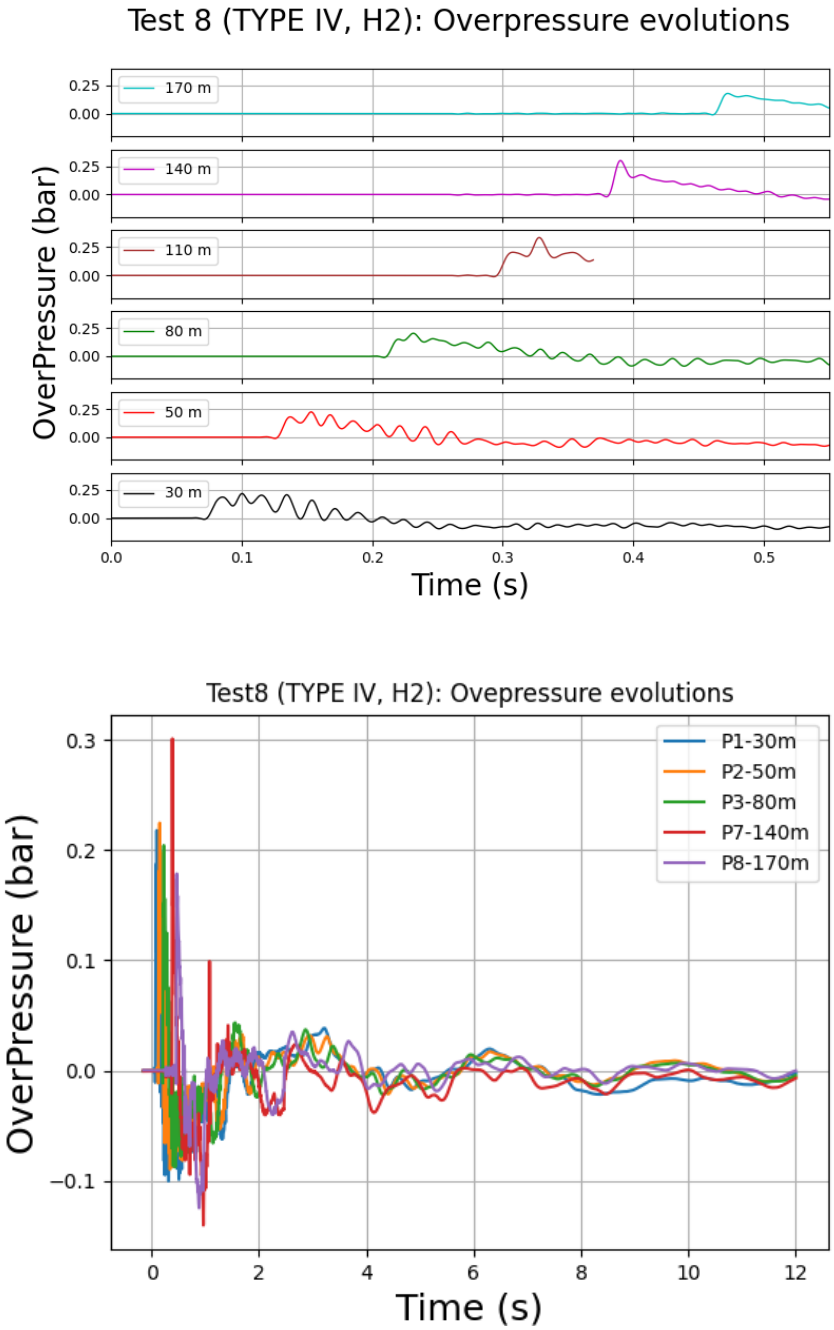

Figure 12: ***Test 8. H2 610 bar, 78L Type IV tank****. Overpressure evolutions at different distances (top), the evolutions are shown for longer time scale (bottom).*

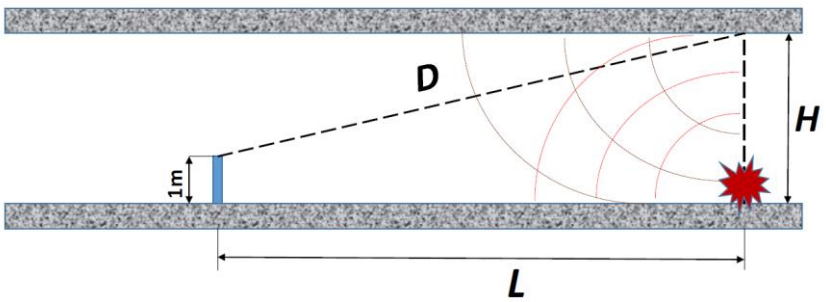

Figure 13: Sketch of the blast wave propagation near explosion zone.

*Table 6 : **Tests 5-8 (Hydrogen tanks).** Maximum overpressures recorded at different distances. The failed transducers are denoted by ----.*

Test	ΔP (mbar) @ 30 m	ΔP (mbar) @ 50 m	ΔP(mbar) @ 80 m	ΔP (mbar) @ 110 m	ΔP (mbar) @ 140 m	ΔP (mbar) @ 170 m	ΔP (mbar) @ 200 m
5	110.4 (136.1)	116.8 (120.4)	113.4	118.2	118.7	----	----
6	101.0	97.7	92.2	100.4	----	84.8	79.8
7	205.0 (271.3)	179.6 (243.2)	160.1 (226.2)	205.5	202.2	----	----
8	187.1 (218.1)	180.5 (224.8)	151.2 (204.4)	205.5 (336.1)	301.3	178.6	----

Finally, in Figure 14 we present the blast wave velocity with respect to distance along the tunnel for the Tests 2, 4 and 8. The velocity values between adjacent pressure transducers are determined using time-of-arrival of the pressure signals and the corresponding distance between the transducers. We can see that, on average, blast waves propagate with a velocity close to 350 m /s. We mentioned in the previous Section that the pencil installed at 80 m from a tank is equipped with two pressure transducers mounted 10 cm apart and denoted P3A and P3B . Based on the data from these transducers, the blast wave velocities are 347 m/s, 350 m/s and 364 m/s for the Tests 2, 4, and 8, respectively.

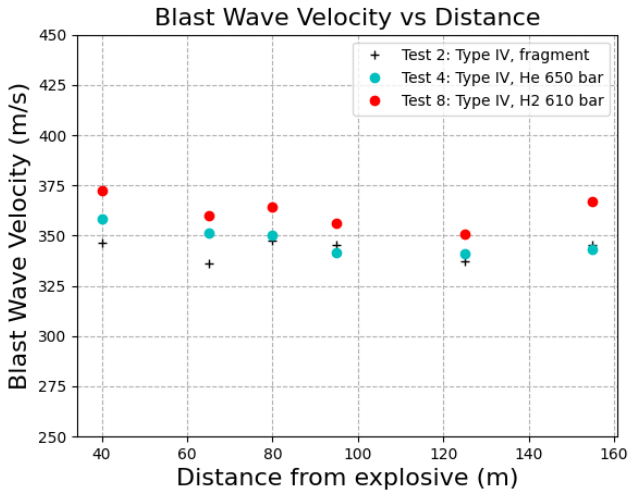

Figure 14 : Blast wave velocity as a function of distance for 3 tests.

Blast wave propagation: analysis

As was mentioned in the Introduction, the energy contained inside a high-pressure hydrogen tank can be split into mechanical energy of compressed gas and chemical energy of combustion when hydrogen is released into air. When the tank is cut open by the action of a detonation belt, the sudden release of pressure generates a relatively strong blast wave in the surrounding air. While this shock wave propagates from the explosion, the hydrogen gas, due to its high post-shock velocity, mixes with air at the contact surface, and a partially premixed combustion

takes place (ignition energy is provided either by a fire or by a detonation belt charge, as in our case). The amount of the premixed hydrogen/air mixture depends on the initial mechanical energy as well as on the surrounding geometry, which can affect the mixing process (via generated turbulence, instabilities, etc.) near the contact surface separating hydrogen from air. Thus a fraction of chemical energy coming from the explosive mixture can be released at relatively fast rate and contribute to the blast wave strength, compared to the rate of chemical energy release during the "fireball phase" represented by a diffusion flame. This mechanism was described in [5], where CFD numerical results on hydrogen filled tanks explosion inside tunnel geometries were carefully analyzed.

The best way to confirm experimentally the fact that a fraction of chemical energy indeed contributes to the blast wave strength is to fill one of the two identical tanks with inert gas (Helium) and the other - with hydrogen gas. If the mechanical energies of these two tanks have close values, the difference in blast wave strengths will serve as a proof of the above statement.

Before proceeding to the comparisons, we shall try to answer the following question: "*What part of mechanical energy contributes to the blast wave strength in case of inert gas filled tank rupture*?" In order answer the question, we performed preliminary analysis related to the contribution of the detonation belt charge to the blast wave strength. The analysis is based on the experimental results of Test 1 and 2 where the DBs were attached to the fragments of each type of tank. The main conclusion is that the contribution of the DB charges to the blast wave strength is relatively small, and does not exceed 5% of the DB energy, equivalent to 48 kJ (Test 2) which is several orders of magnitude smaller than either mechanical or chemical energy contained in tanks. The result is not surprising as most of the energy is used for cutting the tanks.

Helium pressurized tanks: mechanical energy contributing to the blast wave strength

There are several techniques available in order to estimate a blast wave strength from pressurized tank rupture. The overview of these techniques is given in [7] and [4]. Here we shall use the approach of Baker [8], which is based on the numerical studies and the following hypotheses:

- the vessel has spherical form, the effects of the vessel and its fragments are ignored;
- all fluids are assumed to obey equations of state for perfect gases;
- the walls of the tank "disappear" instantly and the flow at the immediate vicinity of the wall is supposed to be one-dimensional at t=0+.

The estimation of the blast wave strength includes two steps. The first step consists of estimation of the initial shock strength p_s using the third hypothesis. In the second step, this value of p_s together with the dimensionless radius of the equivalent volume spherical vessel $\bar{r}_v = r_v(p_s/E_m)^{1/3}$ is employed in order to identify a curve in Figure 17 which provides the values of non-dimensional pressure of the blast wave $\bar{P}$ as a function of the non-dimensional distance $\bar{r}$. Here E_m is the mechanical energy contained in the vessel and obtained using the ideal gas equation of state.

In order to estimate the initial shock strength, Baker [8] used a solution to a shock-tube problem described in [9] and given below

$$\frac{p_1}{p_0} = \frac{p_s}{p_0}\left\{1 - \frac{(\gamma_1 - 1)\,(a_0/a_1)\,\left(\frac{p_s}{p_0} - 1\right)}{\sqrt{(2\gamma_0)\left[2\gamma_0 + (\gamma_0 + 1)\left(\frac{p_s}{p_0} - 1\right)\right]}}\right\}^{\left(\frac{-2\gamma_1}{\gamma_1 - 1}\right)} \tag{1}$$

where p_1, a_1, γ_1 are the pressure, speed of sound and ratio of specific heats corresponding to the compressed gas inside a sphere, while the corresponding values with 0 subscripts corresponds to the properties of surrounding air. This equation can be easily solved for p_s/p_0 by an iterative method, and the results for the initial conditions of the experiments, i.e. $T_0 = 288.15°C$, $\gamma_0 = 1.4$, and $\gamma_1 = 1.667\ (He)$ or $\gamma_1 = 1.39\ (H2)$ are presented in the Figure 15.

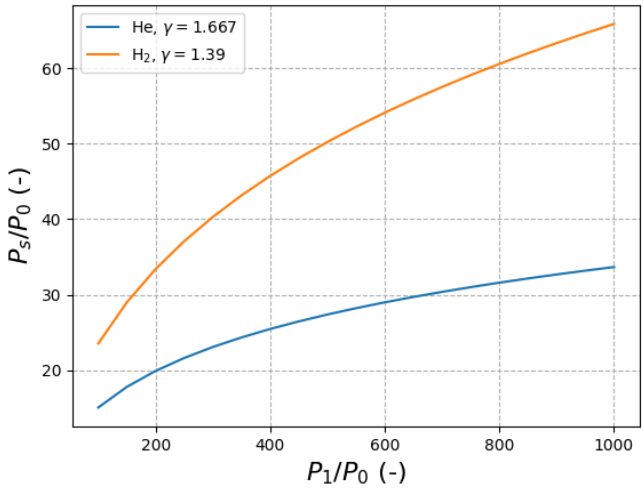

Figure 15 : Values for initial strength of the shock wave.

The hydrogen gas is stored inside conventional tanks at a relatively high pressure, and if we need to estimate the corresponding mass or mechanical energy of the compressed hydrogen gas, a real gas equation of state has to be applied. The Noble-Abel equation of state is widely used for high storage hydrogen or helium gas pressures [4]:

$$p(v - b) = \frac{\bar{R}\,T}{M}, \tag{2}$$

where $v = \frac{1}{\rho}$, b is the co-volume constant, $\bar{R}$ is the universal gas constant, and M is the molar mass of the compressed gas. Will the result differ much from those presented in Figure 15 if we use the Noble-Abel equation of state inside a vessel, instead of the Ideal gas equation of state?

The solution to the shock tube problem in general form for Noble-Abel Stiffened Gas equation of state is presented in recently published paper [10].

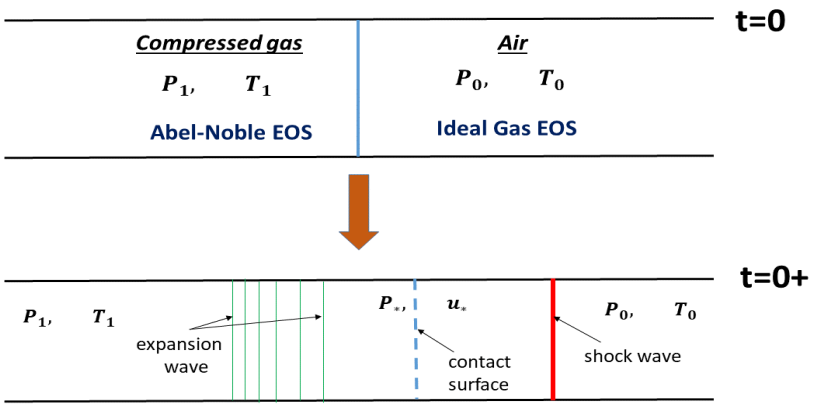

Figure 16 : Sketch of a shock tube problem with used notation.

We can assume that the surrounding air satisfies the ideal gas equation of state as the pressure levels of the initial shock wave does not exceed 100 bar (Figure 15). The sketch of the shock tube problem is given in Figure 16, where a shock wave propagating into air with corresponding shock Mach number M_s and an expansion wave sweeping the compressed gas are depicted. The pressure as well as the velocity are constant across the contact surface and denoted as p_* and u_*, respectively.

We simplify the general formulation of [10] by taking into account only the co-volume constant b_1 of the Noble-Abel equation of state.

$$\frac{2}{\gamma_1 - 1}\sqrt{\gamma_1 p_1 (v_1 - b_1)}\left(1 - \frac{p_*}{p_1}\right)^{(\gamma_1 - 1)/(2\gamma_1)} - u_* = 0 \tag{3}$$

$$\frac{p_*}{p_0} = 1 + \frac{2\gamma_0 \left(M_S^2 - 1\right)}{\gamma_0 + 1} \tag{4}$$

$$\frac{u_*}{c_0} = \frac{2(M_S^2 - 1)}{(\gamma_1 + 1)M_S} \tag{5}$$

The Equations (3)-(5) constitute a system which can be transformed into a non-linear equation for M_s. Interesting fact is that these equations give exactly the same solution for the strength of the shock wave as the Equation (1). The reason lies in the form of Equation (3), where the only contribution of the "non-ideal" gas is $(v_1 - b_1)$ which, using the Equation (2), is equal to $\bar{R}T_1/(M_1 p_1)$. The latter value is obtained using the measured values. In other words, the solution given by Baker [8] is still valid for high-pressure gas vessels! The only problem lies in the fact that non-dimensional distance $\bar{r}$ is computed using the mechanical energy based on ideal gas equation of state.

As the next step, the obtained value for p_S is used in order to determine the evolution of non-dimensional overpressure as a function of non-dimensional distance $\bar{r}$ using the Figure 17 where the Figure from [8] is extrapolated to lower non-dimensional overpressure values in the spirit of [4].

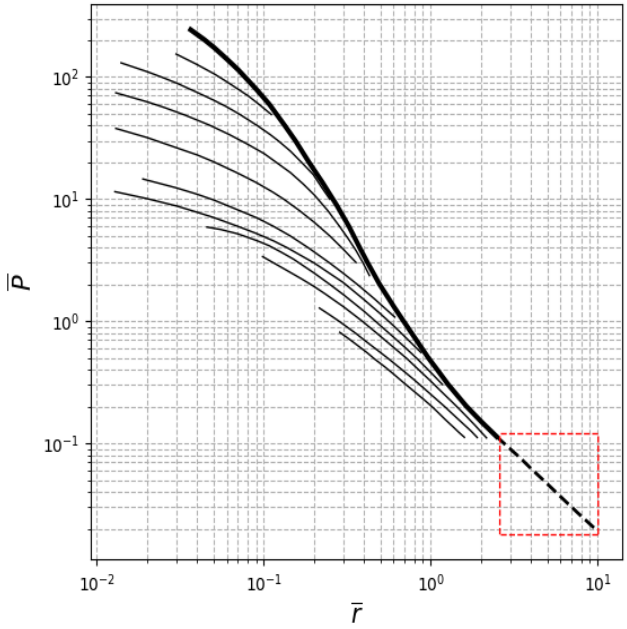

Figure 17 : non-dimensional overpressure $\bar{P}$as a function of non-dimensional distance $\bar{r}$ (Scanned from [8]).The extrapolated part is shown inside the red box.

Due to the fact that the experimental results are obtained inside the tunnel, we cannot use directly the curve of the Figure as these computational results are obtained for spherical vessels in the open atmosphere above the ground. We shall apply the technique of Silvestrini [3] in order to proceed. The technique implies the concept of energy concentration factor (ECF) which is the ratio of volumes of the explosion hemisphere and the tunnel. The mechanical energy is multiplied by a factor 1.8 due to a fact that the tanks were located at the ground level [8]. The closest measurement point from the explosion is 30 m. In our experimental configuration this corresponds to

$$ECF = \frac{V_{hem}}{V_{tun}} = \frac{1}{3}\frac{\pi r^2}{A_{tun}} = \frac{1}{3}\frac{\pi \cdot (30m)^2}{41.35m^2} = 22.8 \qquad (6)$$

For the Helium tests 3 and 4 this corresponds to the non-dimensional distances:

$$\bar{r}_3 = r \cdot \left(\frac{p_s}{ECF \cdot 1.8 \cdot E_m}\right)^{\frac{1}{3}} = 30m \cdot \left(\frac{0.87 \cdot 10^5 Pa}{22.8 \cdot 1.8 \cdot 1.283MJ}\right)^{\frac{1}{3}} = 3.53,$$

$$\bar{r}_4 = r \cdot \left(\frac{p_s}{ECF \cdot 1.8 \cdot E_m}\right)^{\frac{1}{3}} = 30m \cdot \left(\frac{0.87 \cdot 10^5 Pa}{22.8 \cdot 1.8 \cdot 5.882MJ}\right)^{\frac{1}{3}} = 2.13,$$

where the mechanical compression energy was calculated using the Noble-Abel equation of state.

Looking at the Figure 17 : non-dimensional overpressure $\bar{P}$as a function of non-dimensional distance $\bar{r}$ (Scanned from).The extrapolated part is shown inside the red box. We notice that this distance corresponds to the extrapolated part of the overpressure evolution. Baker in his

work [8] indicated that the curves corresponding to this Figure have uncertainty of $\pm 20\%$. Due to the fact that the curve is extrapolated we shall increase uncertainty to $\pm 25\%$ in this area.

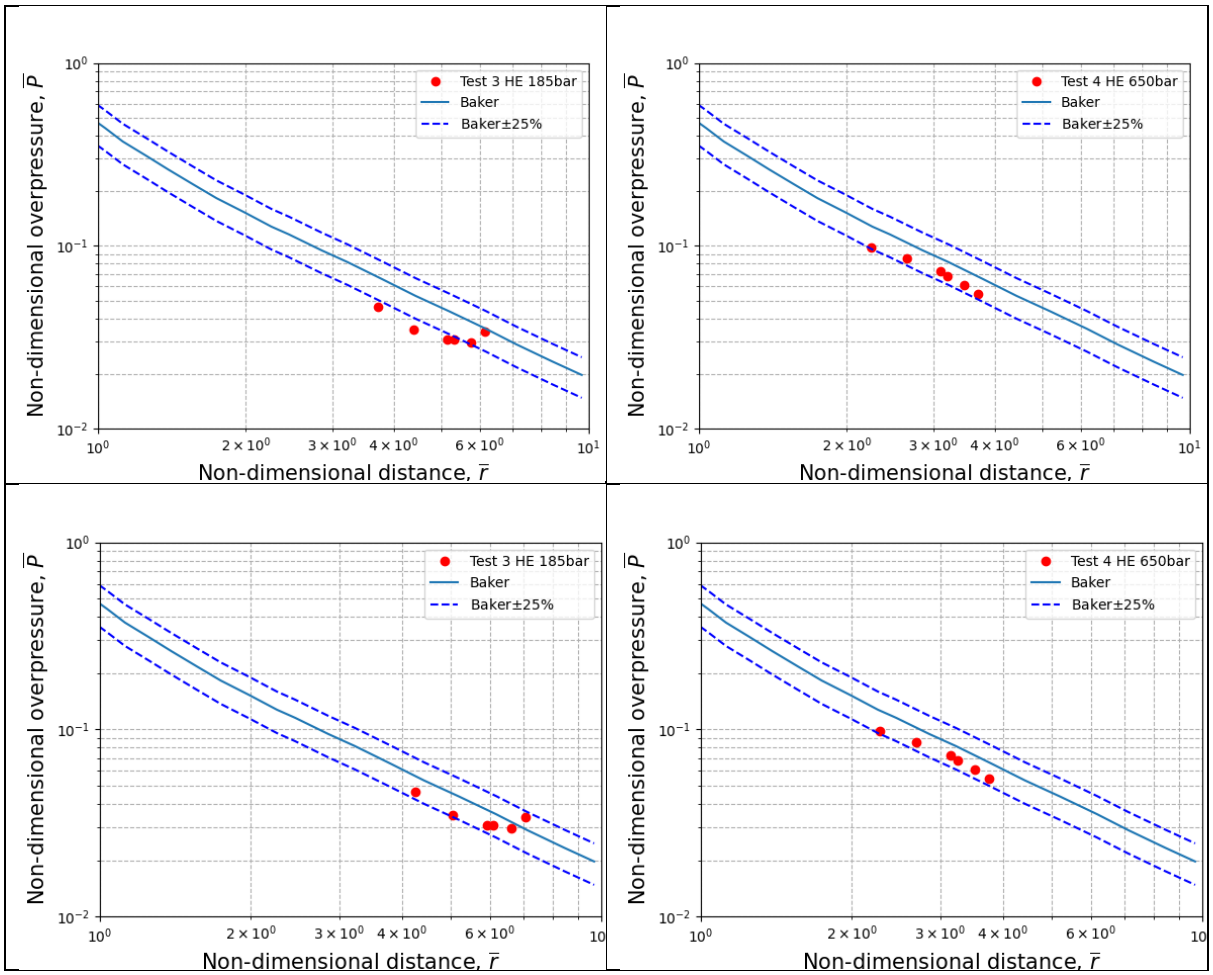

Figure 18 : Comparaison of the experimental data for Tests 3 and 4 with the results from [8]. 100% of mechanical energy is used (top) and fraction of mechanical energy (68%) (bottom).

At first, the total amount of mechanical energy E_m is taken into account and the comparisons between the extrapolated curve of [8] and the experimental data for maximum overpressure are presented at the upper part of Figure 18 (Test 3, left; Test 4, right). We can see that the results corresponding to the Test 4 lie almost entirely inside the uncertainty region, while most of the points of the Test 3 lie outside this region. By modifying the percentage of mechanical energy contributing to the blast wave strength we arrive at the results presented in Figure 18, bottom, where we take 68% of E_m (Test 3) and 95% of E_m (Test 4).

Estimation of the kinetic energy of fragments.

The used tanks of Type II has the following characteristics: mass = 60.5 kg; length = 1.45 m, and of Type IV: mass = 64.6 kg, length = 0.96 m. Again, using the results of Baker (Figure 5.3 of [8]) we deduce that the initial velocity of each fragment is 34.4 m/s (Test 3) and 98.2 m/s (Test 4). Taking into account the mass of the fragments, we arrive at the following estimation: $E_{cin} = 2.8\%\ E_m$ (Test 3), and $E_{cin} = 5.3\%\ E_m$ (Test 4). That means that only a small fraction of the mechanical energy is spent on projection of the fragments.

To be on the conservative side, we take in the following analysis all mechanical energy in the case of hydrogen-filled tanks.

Hydrogen pressurized tank: energy contributing to blast wave strength

It is emphasized in [4] and [5] that a certain amount of chemical energy has to be taken into account in order to model the blast wave pressure decay due to high pressure hydrogen tank explosion. Moreover, a method to define the contribution of the chemical energy was developed in [5]. The method is based on a physical argument that the contribution of combustion to the peak overpressure stops when the temperature gradient along the tunnel changes from negative to positive value thus preventing acoustic waves from reaction zone propagate and reach the blast wave front. Based on this technique and under assumptions of the modelling, it was shown in [5] that approximately 12% of chemical energy contribute to the blast wave strength.

Using the obtained experimental data, we shall demonstrate that, indeed, a certain amount of chemical energy contributes to the blast wave strength. If it were not true, than two identical tanks, initially filled with helium and hydrogen and having similar mechanical energy, would give similar values of maximum overpressure after explosion. Unfortunately, the amount of energy contained inside helium-filled tanks is not exactly the same as the amount of mechanical energy contained in hydrogen-filled tanks. We therefore proceed in the following way.

We consider two groups of tests (Tables 7 and 8). In each group, two tanks are filled with hydrogen gas, and one tank is filled with helium gas. The corresponding mechanical energies are such that the helium-filled tank energy is intermediate between two hydrogen-filled tank energies; 100% of mechanical energy is considered for all cases. If a blast wave strength were based solely on mechanical energy of compressed gas, the maximum overpressure evolution with distance corresponding to the helium-filled tank would be sandwiched between the corresponding overpressures of the hydrogen-filled tanks.

Table 7 : First group of tests.

Test N°	Tank	Pressure (bar)	Temperature, °C	Mechanical Energy, MJ	Gas
20	TYPE II	47	10	0.56	Hydrogen
3	TYPE II	185	15	1.28	Helium
5	TYPE IV	90	15	1.60	Hydrogen

Table 8 : Second group of tests

Test N°	Tank	Pressure (bar)	Temperature, °C	Mechanical Energy, MJ	Gas
6	TYPE II	194	15	2.09	Hydrogen
4	TYPE IV	650	15	5.88	Helium
7	TYPE IV	520	15	7.39	Hydrogen

The experimental results corresponding to each group of tests are presented in Figure 19 and Figure 20, respectively. In both cases, *helium-related results for maximum overpressure are lower than the results corresponding to hydrogen-filled tanks*. Moreover, the slopes of the best-fit lines corresponding to the helium-filled tanks have lower values than the slopes

corresponding to hydrogen-filled tanks. The slopes of the best-fit lines (in log-log scales) corresponding to the Tests 20, 3 and 5 are -0.188 mbar/m, **-0.197** mbar/m, and -0.0853 mbar/m, respectively; and the slopes of the best-fit lines corresponding to the Tests 6, 4 and 7 are -0.077 mbar/m, **-0.323 mbar/m** and -0.196 mbar/m, respectively.

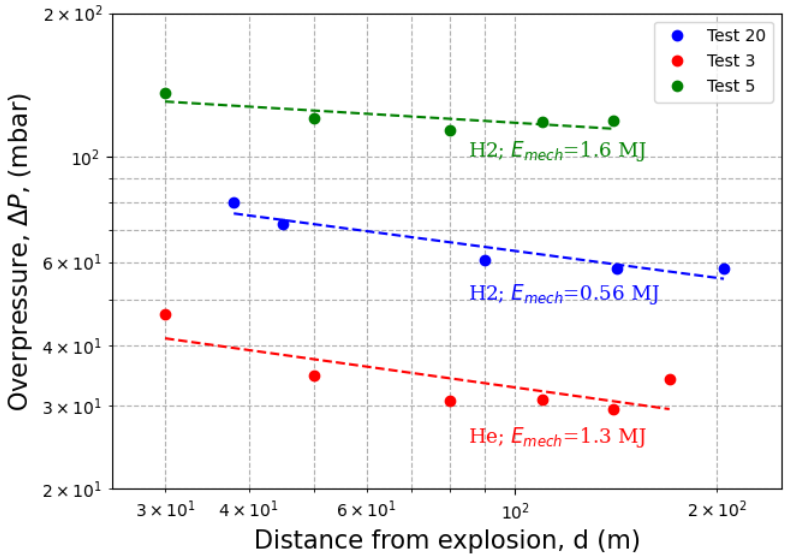

Figure 19 : Results for maximum overpressure decay along the tunnel corresponding to the first group of tests.

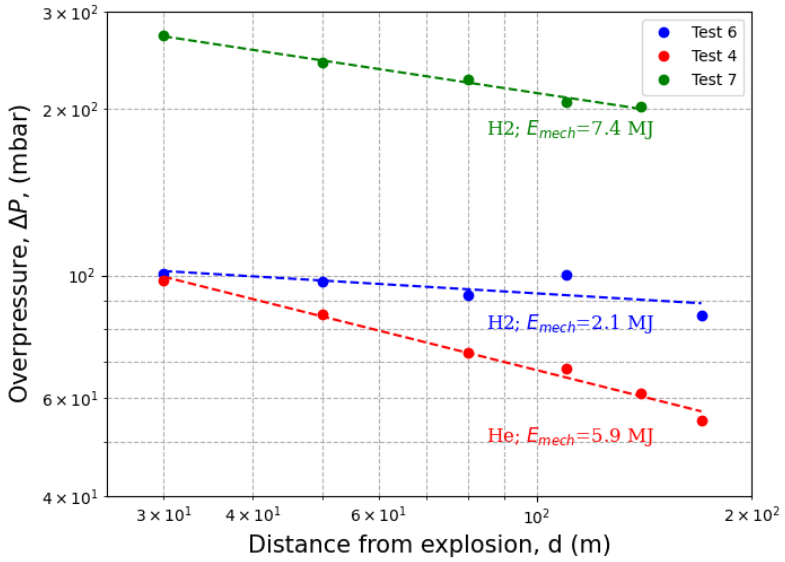

Figure 20 : results for maximum overpressure decay along the tunnel corresponding to the second group of tests.

The above results confirm the findings of [4] and [5] that a fraction of chemical energy contributes to the blast wave strength. The open question remains as of the value of this fraction. We speculate that this value strongly depends on two factors: the mechanical energy of the compressed hydrogen and the surrounding geometry (tank is isolated or located inside a car, etc.). In what follows, we shall compare our experimental results with the only available correlation for pressure decay inside a tunnel [5].

The paper [5] presents a universal correlation for blast wave decay after hydrogen tank rupture in a tunnel fire. This correlation was developed using methods of similitude analysis and numerical experiments. In terms of energy, the total mechanical energy contained in the tank as well as the fraction of chemical energy (12% in the paper) is accounted for.

The best fit line for the universal correlation is:

$$\bar{P}_T = 0.22 \cdot \bar{L}_T^{-1.35} \tag{7}$$

while the conservative form of the correlation is:

$$\bar{P}_T = 0.87 \cdot \bar{L}_T^{-1.35} \tag{8}$$

The above correlation is expressed in terms of non-dimensional distance $\bar{L}_T$ and non-dimensional overpressure $\bar{P}_T$, where

$$\bar{L}_T = \frac{p_0 L A_T}{E \cdot AR^{0.5}} \cdot \frac{fL}{D_T} \text{ , and } \bar{P}_T = \frac{\Delta P}{p_0 \bar{L}_T}.$$

The following values are taken for the analysis:

- Atmospheric pressure: $p_0 = 0.87\ bar$;
- Tunnel cross-section area: $A_T = 41.3\ m^2$ (L < 87 m), and $A_T = 33\ m^2$ ($L > 87\ m$)
- Friction factor: f = 0.0055
- Aspect ratio: AR = 1.6 (L < 87 m), and AR = 1.4 (L > 87 m)
- Hydraulic diameter: $D_T = 6.6\ m$ (L < 87 m), and $D_T = 6.0\ m$ (L > 87 m).

The tests used for comparisons are presented in Table 9. One set of data from the pretest campaign of 2020 (Test 20), rupture of Type II tank of 50 L containing hydrogen at 47 bar, is added to the plot. The results were reported earlier [6]; here we give the maximum overpressure levels, for completeness (Table 10). The mechanical energy is computed using Noble-Abel equation of state of a real gas with constant $b = 7.69 \times 10^{-3} \frac{m^3}{kg}$. For further analysis, we consider 180% of the mechanical energy and 12% of the chemical energy, i.e.

$$E = 1.8 \cdot E_M + 0.12 \cdot E_{CH} \tag{9}$$

We assume here that all energy of a DB is spent on a tank rupture.

The results are given in Figure 21 (only the first overpressure peak is taken into account) and Figure 22 (the second overpressure peak is taken into account). We can see that most of the data are below the best fit line of the correlation. The best fit line corresponding to the present results (in red color in Figure 22) has a slope value of -1.24, which is close to the slope value of -1.35 obtained in [5]. We mention that taking different (from 0.12) fraction of the chemical energy does not change the best-fit slope of the experimental results.

Table 9 : The tests used for comparison. The mechanical and chemical energies are given

Test N°	Tank	Pressure (bar)	Temperature, °C	Hydrogen Mass, kg	Mechanical Energy, MJ	Chemical Energy, MJ
5	TYPE IV	90	15	0.56	1.60	66.92
6	TYPE II	194	15	0.73	2.09	86.94
7	TYPE IV	520	15	2.55	7.39	306.14

8	TYPE IV	610	15	2.87	8.31	344.13
20	TYPE II	47	10	0.2	0.56	24.41

Table 10 : Maximum overpressure values measured at different distances for pre-Test 20

Test	ΔP (mbar) @ 38 m	ΔP (mbar) @ 45 m	ΔP(mbar) @ 90 m	ΔP (mbar) @ 142 m	ΔP (mbar) @ 205 m
20	80.0	72.1	60.5	58.2	58.1

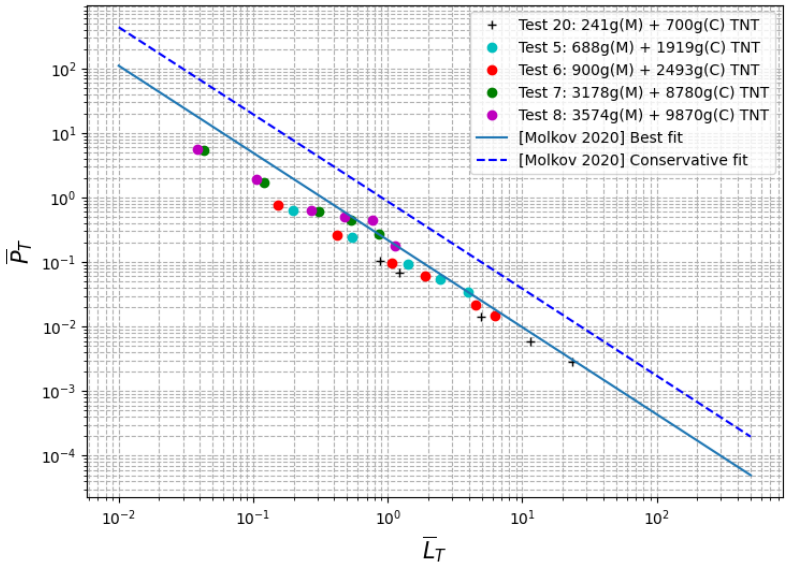

Figure 21: Comparison of experimental data with universal correlation [5]. First peak of pressure is taken into account. (M) stands for "Mechanical Energy", (C) stands for "Chemical Energy".

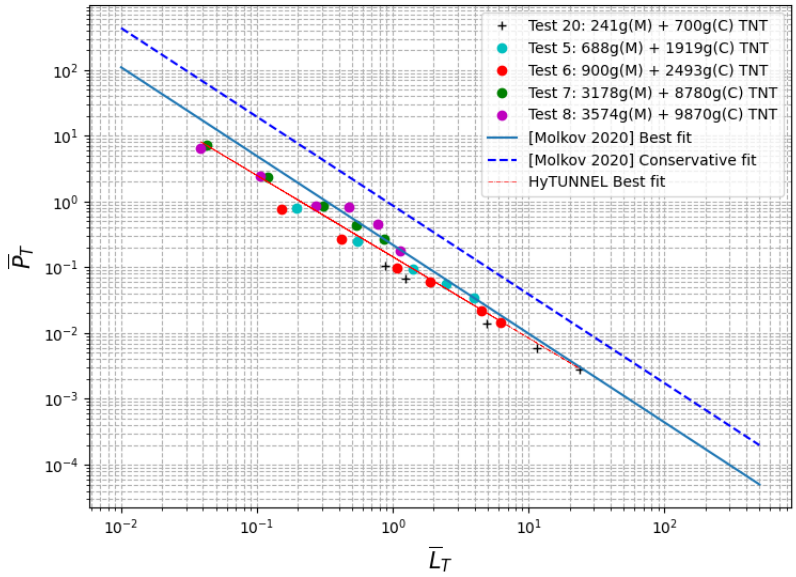

Figure 22: Comparison of experimental data with universal correlation. Second peak of pressure is taken into account. (M) stands for "Mechanical Energy", (C) stands for "Chemical Energy".

We have varied the fraction of chemical energy in order to minimize the distance between the best-fit curve and our results. The minimal distance corresponds to 5% of chemical energy input (see Figure 23). Let us take one of the experimental points closest to the best-fit curve; consider the point at $\overline{L}_T = 0.94$ corresponding to the Test 7 (green color on the Figure). Using Formulae (7) and (8) we arrive at the overpressure values: $\Delta P = 0.196\ bar$ (best fit) and $\Delta P = 0.773\ bar$ (conservative fit). The conservative estimation gives overpressure value that is nearly four times higher than the one corresponding to the best-fit curve.

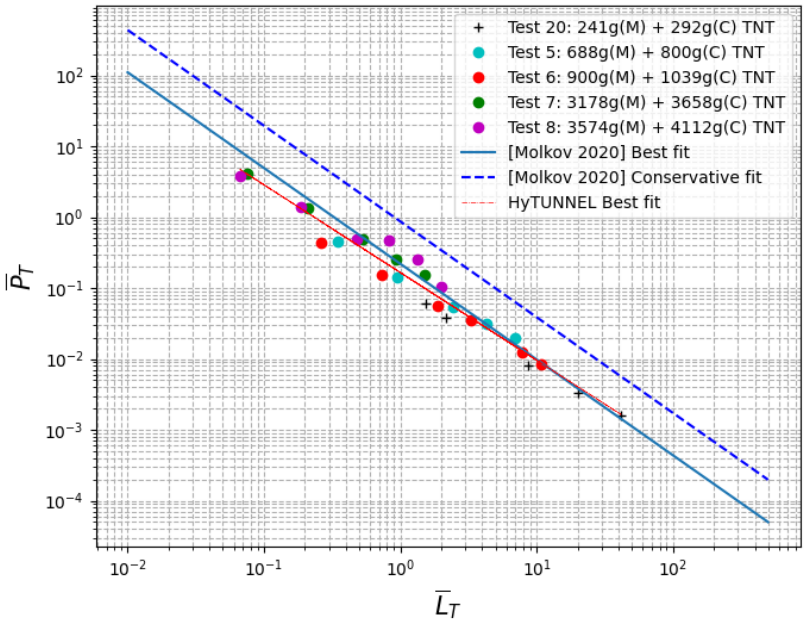

Figure 23 : Comparison of experimental data with universal correlation. Second peak of pressure is taken into account. (M) stands for "Mechanical Energy", (C) stands for "Chemical Energy". 5% of chemical energy is taken into account.

The impulse is another important parameter describing blast waves. We can expect that the impulse values are more important inside a tunnel, compared to an open space, due to energy concentration phenomenon. Ideally, it would be interesting to compare blast wave characteristics (maximum pressures and impulses) of hydrogen-filled tanks having identical energy contents, and one being exploded in open space, while the other – inside a tunnel. Zalosh and Weyandt [1] described an explosion of hydrogen-filled tank in an open atmosphere. The hydrogen pressure and temperature at failure were 357 bar and 39°C. If we consider the amount of energy computed via Equation (9), i.e. 180% of the mechanical energy and 12% of chemical energy, this would give for energy the value of 33.0 MJ. Thus computed energy values of closest tests, Test 6 and Test 7, are 14.2 MJ and 50.0 MJ, respectively.

We scanned the overpressure curves corresponding to the hydrogen tank explosion in open space described in [1]. The considered overpressure curves are those corresponding to distances 4.2 and 6.5 m. The corresponding values of impulses are: 8.5E-4 $bar \cdot s$ and 8.3E-4 $bar \cdot s$. The impulse values at different distances for Tests 6 (192 bar, H2) and 7 (520 bar, H2) are given in the Table 11. Only the positive phases of the overpressure evolutions are taken into account.

Table 11 : Impulse values at different distances for Test 6 and Test 7.

Test \ Impulse at (bar * s)	30 m	50 m	80 m	110 m	140 m	170 m	200 m
Test 6	5.2E-3	5.7E-3	5.6E-3			4.3E-3	2.6E-3
Test 7	1.3E-2	1.2E-2	1.3E-2	1.8E-2	1.1E-2		

We can see that even the impulse values corresponding to the Test 6, having twice-smaller amount of energy and measured at much longer distances, one order of magnitude bigger than those corresponding to test of [1].

In order to present the results on a Figure, we form non-dimensional variables according to [8] (Equations (9) and (10)). Corresponding Energy Concentration Factors multiply the energy values corresponding to the Test 6 and Test 7, as it was done earlier (Equation (6)). The results are plotted in Figure 24 together with a curve for impulses in open space scanned from [8]. Again, the results show that the impulses corresponding to the tests in tunnel have much larger values. Another observation is that one needs an impulse-vs-distance correlation corresponding to high-pressure gas tank explosion in a tunnel, as the correlation of [8] poorly represent experimental data.

$$\bar{I} = \frac{I \cdot a_0}{E^{\frac{1}{3}} \cdot p_0^{2/3}} \tag{9}$$

$$\bar{r} = r\left(\frac{p_0}{E}\right)^{\frac{1}{3}} \tag{10}$$

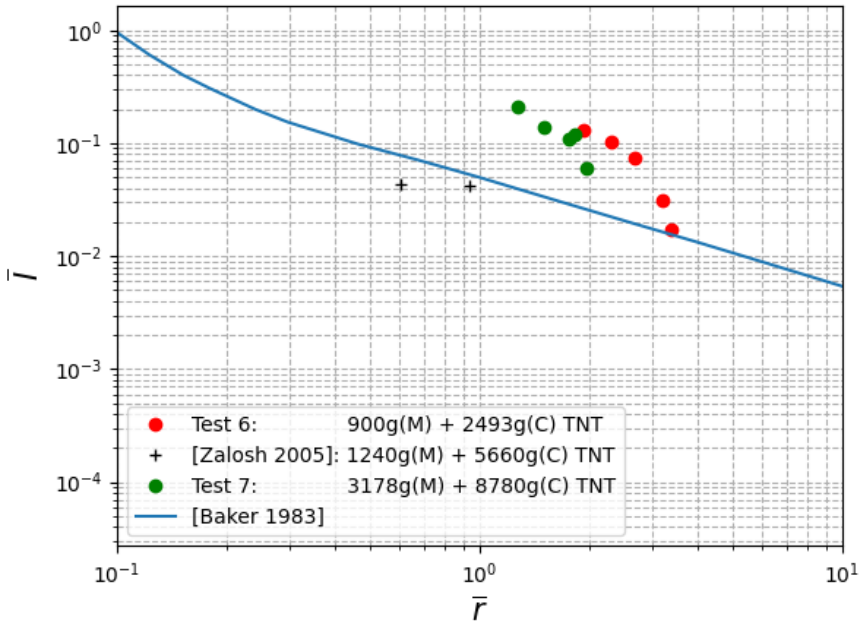

Figure 24 : Comparison between non-dimensional impulse values corresponding to Test 6, Test 7 and the experimental data of [1].

Fireball evolution: experimental data and analysis

It is evident that the tests relevant for fireball analysis are only those in which the tank is pressurized with hydrogen. Two high-speed cameras (Phantom Miro M310) operated at 10000 fps were located at about 100 m from the explosion in a protective box to record the shape of the fireballs.

The fireball behavior in a tunnel is expected to differ from its behavior in an open area. This is due to geometrical constraints of the tunnel. First, a fireball projection cannot exceed the tunnel cross-section. Second, the blast waves from the compressed gas, being reflected from the tunnel lateral walls, slow down the propagation of the reaction zone due to reverse gas velocities. This can result in an oscillatory behavior of the reaction zone. This phenomenon, observed in one of the 2020 pre-tests, is depicted in Figure 25: an explosion of tank of Type II filled with 36 bar of hydrogen and 5 bar of helium gas was filmed.

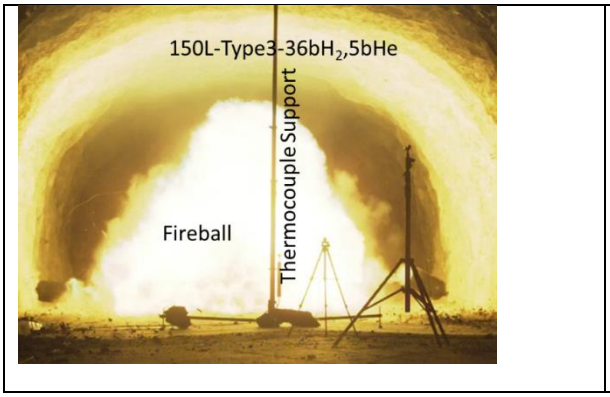

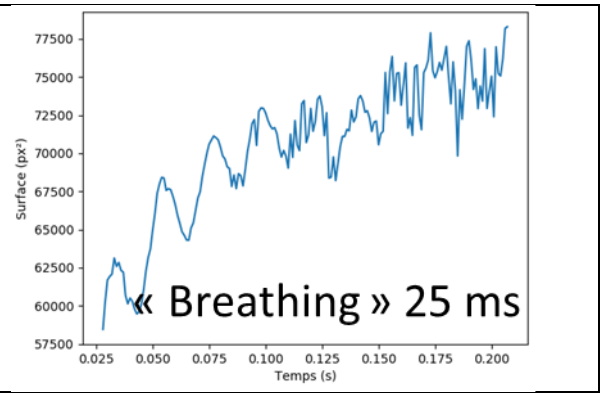

Figure 25 : 2020 pre-test. Left: fireball picture, Right – result of post-treatment of fireball surface.

The image processing method is explained in Figure 26. This method is based on a threshold gray levels image and contour detection. It is inherently a 2D process and the tools are programmed in Python using the OpenCV toolbox. The processed fireball surface projection evolution is given in Figure 25 (right). The "breathing" of the fireball can be clearly seen and the period is close to 25 milliseconds. It probably corresponds to a mixture of the sound velocities in the fresh and burnt gases brought back to the radius of the tunnel. This phenomenon probably has also an impact on the turbulent velocities to be used to calculate these fireballs in a confined environment.

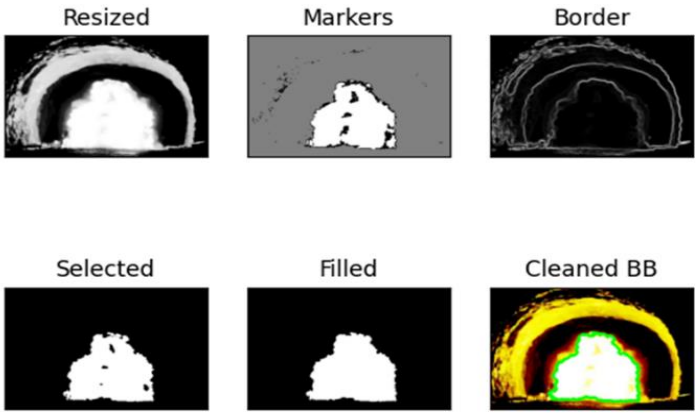

Figure 26 : Post-processing method to derive the fireball surface.

We mention that the "breathing" behavior of fireball was observed numerically while modelling a hydrogen filled tank explosion in a tunnel by Ulster University [11].

Morphology of the fireballs

It is mentioned before that a fireball can fill completely a tunnel cross-section provided the pressure inside a tank is sufficiently high. Among four presented tests, two (Test 7 and 8) resulted in fireballs which fill the tunnel section at particular time. Here we present fireball evolution corresponding to Test 5 (Figure 27; cross-section is not filled) and Test 8 (Figure 28; cross-section is filled).

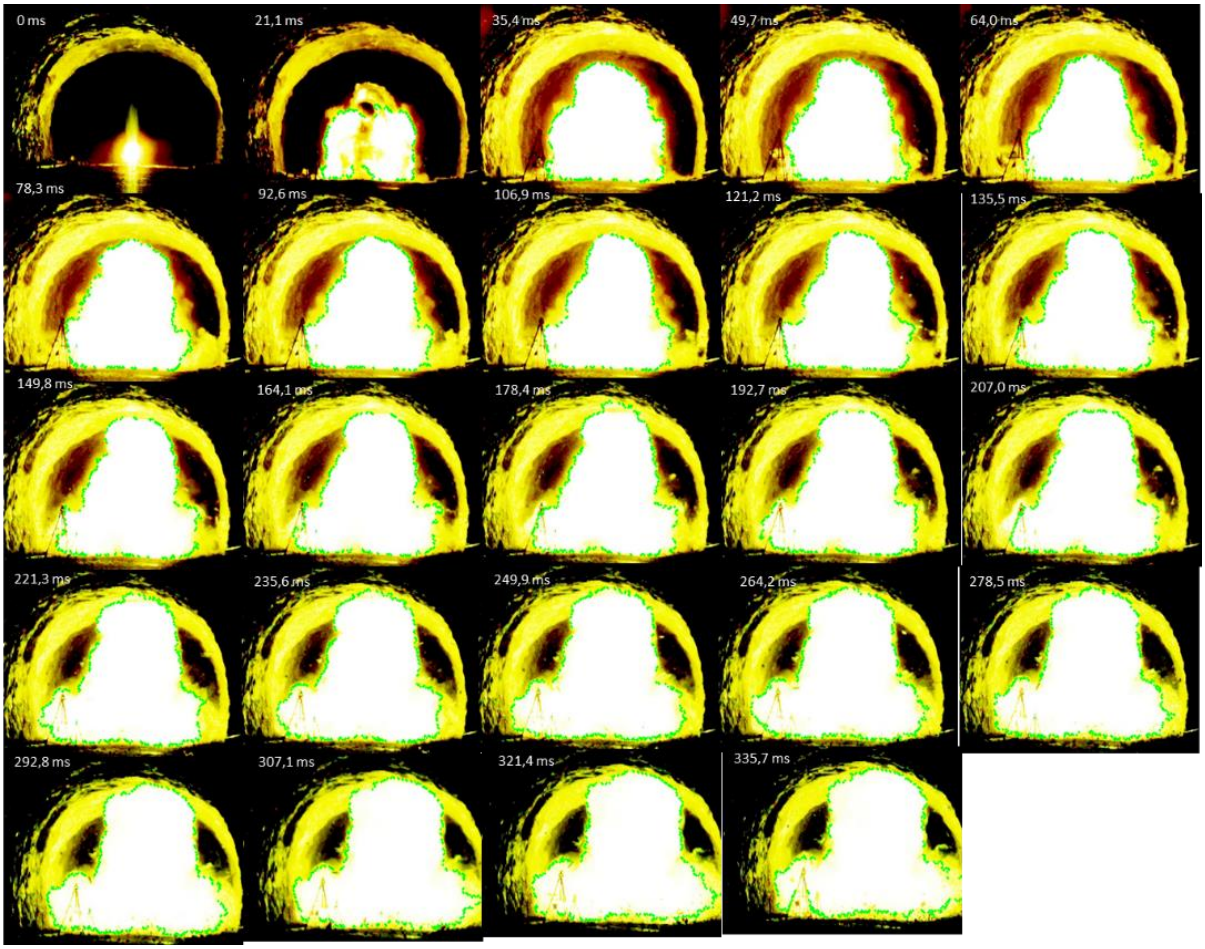

Figure 27 : Test 5. Fireball evolution with time.

On the images of the fireball of Test 5 (90 bar, Figure 27), one can see that the first glow comes from the ignition of the solid explosive initiating the explosion of the detonation belt. Then, the fireball is square-shaped because of the specific shape of the detonation belt focusing the waves for the circumferential cutting of the tank. From 20 ms, the luminosity increases and the chemical reaction with hydrogen starts. At the beginning, a hemispherical ball develops. Then (60 ms), the reaction progresses with the two fragments of the tank which are expelled violently towards the side walls, while the remainder of the fireball is slowed down by the pressure waves which reflect on the walls. In this test, the fireball does not spread over the entire cross-section of the tunnel.

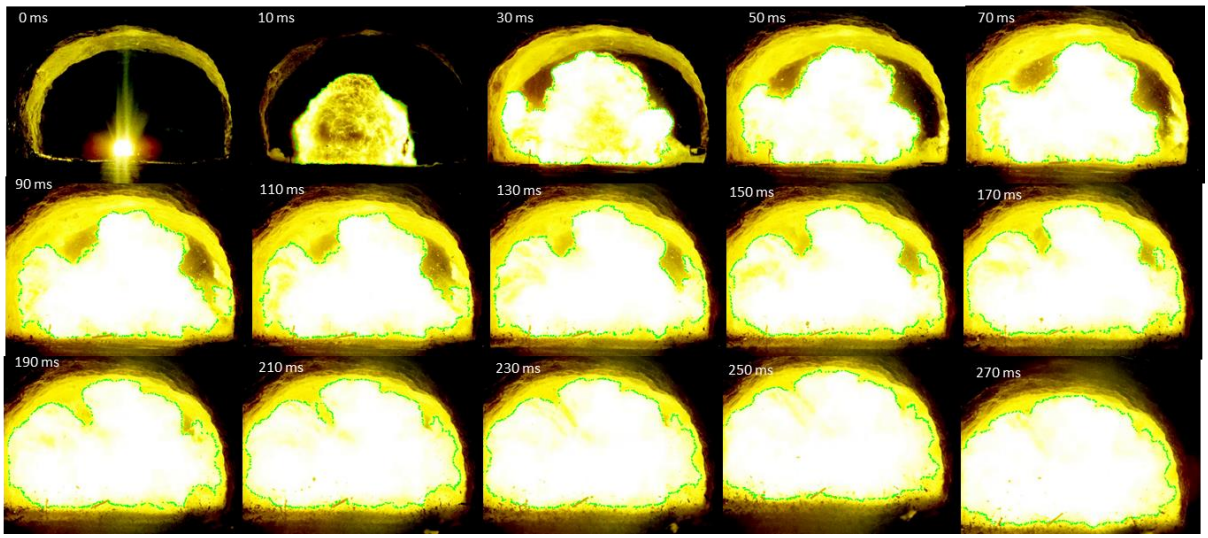

Figure 28 : Test 8. Fireball evolution with time.

The next test, Test 8 (Figure 28) was carried out with a Type IV tank of 78 liters and internal pressures of 610 bar. The phenomena observed are relatively identical. The sequence of stages accelerates, the fireball is already luminous and hemispherical from 10 ms. Then, it progressively engulfs the whole cross-section of the tunnel. In the last image of Test 8, the box containing the camera starts to move under the effect of the blast waves (270 ms).

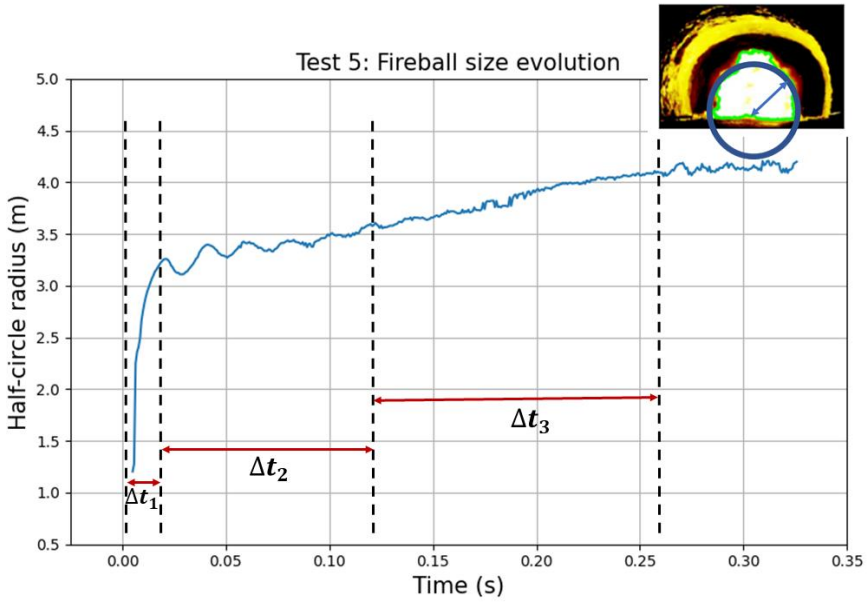

Figure 29 : Test 5. Fireball size evolution in terms of half-circle radius.

The surface of the fireball can be translated into a radius of an equivalent hemisphere (Figure 29, top right). On the Figure 29 we present an evolution of the radius of the hemisphere corresponding to the fireball scenario of the Test 5. Different behaviour patterns can be distinguished by looking at the curve. First, a relatively high increase of the half-circle radius, which lasts about $\Delta t_1 \approx 10 - 20ms$, is observed. This period is followed by a "breathing", or oscillatory, behaviour of the fireball with diminishing amplitude with time; it is approximately

one order of magnitude longer, i.e. $\Delta t_2 \approx 100ms$. As was mentioned before, this step is unique to the tunnel geometry and cannot be observed in the open area. The third period, which lasts about $\Delta t_3 \approx 150 - 200ms$, correspond to a linear growth of the fireball. During the fourth period, the fireball area stabilises at some value, which is either lower than the maximum value corresponding to the tunnel cross-section area, or is equal to this value (fireball fills completely the area).

In Figure 30 we present evaluated fireball evolution scenarios for Tests 5-8. We can see that the curves behave likewise, i.e. the three elements described above can be clearly distinguished. The differences between the Tests lie in the oscillation period, which varies between 17 ms (Test 8) and 20 ms (Test 5), as well as in the linear growth rate, varying between 2.3 m/s (Test 7) and 4.4 m/s (Test 5).

We mention that the method based on CFD analysis was developed in [5] in order to define a fraction of chemical energy contributing to the blast wave strength. The analysis led to the conclusion that the chemical energy contributes to the overpressure during relatively short time scale, of the order of, or below 10 ms. Interestingly, this time scale corresponds to the first part of the scenario, i.e. to the period of fastest-growing fireball.

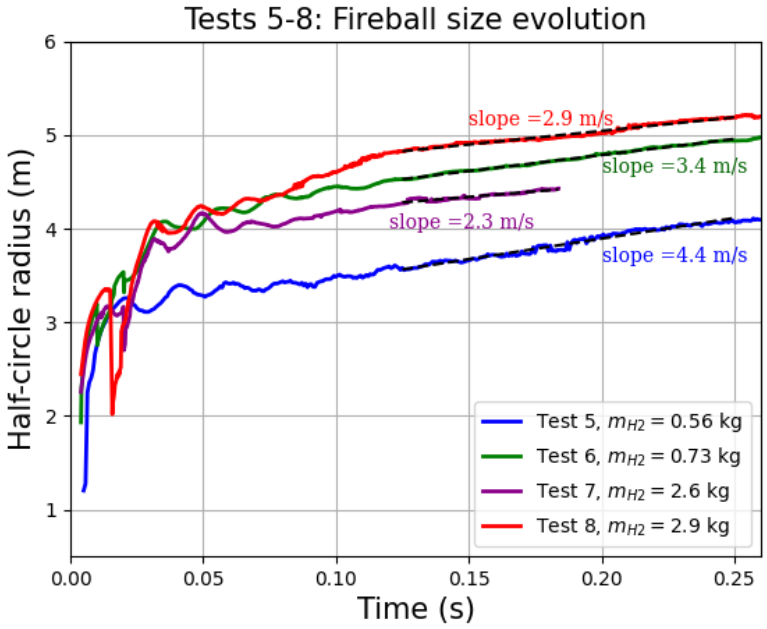

Figure 30 : Tests 5-8. Fireball size evolution.

In the literature, size of fireballs produced by hydrogen tanks put in a fire are also reported from different publications. Makarov et al [12] have recently published a review on this subject. They gathered different experimental data and proposed theoretical and conservative correlations to estimate the equivalent hemispherical radius:

$$r_{hms} = 4.9 \cdot m_{H2}^{\frac{1}{3}} \ (theor.) \quad r_{hms} = 9.75 \cdot m_{H2}^{\frac{1}{3}} \ (conserv.)$$

Zalosh et al. [1] also presented experimental data about fireball size and duration *t* of fireball event in the form of different correlations whereas the buoyancy or convection are dominant phenomena:

$$r_{hms} \sim 5 \cdot m_{H2}^{1/3}$$

t=0.47 $m_{H2}^{1/3}$ in convection dominated regime and
t=2.6 $m_{H2}^{1/6}$ in buoyancy dominated regime.

The correlation for the fireball size is very similar to the theoretical correlation of [12].

Application of these correlations to the 2021 test conditions leads to fireballs greater than the dimensions of our tunnel if we consider the conservative one. However, the theoretical correlation of [12] and the one of [1] lead a fireball smaller than the tunnel diameter for the first two test conditions (Tests 5 and 6). The two other tests will lead to fireballs filling completely the tunnel cross-section. The durations varies from 0.5 to 3 seconds depending on the convective or buoyant dominant expansion process.

Table 12 :Global characteristics of the fireball Tests 5-8. The fireball dimensions are computed using the formulae from [1] and [12] (theoretical)

Volume	Pressure (bar)	Mass H_2 (kg)	$R_{hem.}$ (m) [1] – [12]	t (s) conv -buoy	Test n°
50	194	0.725	4.5 – 4.4	0.4 – 2.5	n°6
78	90	0.558	4.1 - 4.0	0.4 – 2.4	n°5
	520	2.554	6.8 – 6.7	0.6 – 3.0	n°7
	610	2.871	7.1 - 7.0	0.7 – 3.1	n°8

The above comparisons, however, have to be taken with caution, since the available correlations were obtained in open areas while the present experimental data are affected by the tunnel geometry. Another point is that the obtained in the tunnel fireball characteristics are measured solely inside the tunnel “cross-section” dimension, and for complete analysis, one needs the fireball evolution along the tunnel axis.

4. Conclusions

This document details the results obtained during tank rupture experiments in the Mortier road tunnel. Two tests have been performed with helium gas inside (Test 3 and Test 4), five tests – with hydrogen filled tanks (Tests 5-8 and Test 20) and two tests with empty tanks (Tests 1 and 2). The hydrogen gas pressure varied between 90 bar and 610 bar. The detonation belt charge is kept constant for each tank Type, its energy is given in TNT equivalent units, i.e. 130 g for tank of Type II and 228 g for tank of Type IV. Seven PCB blast wave pencils were installed in the tunnel in order to capture the pressure waves. The signals were analyzed in terms of maximum overpressures. The main results show that:

- Concerning the tests with fragment and detonation belts (Test 1 and 2), maximum overpressure levels are lower than 20 mbar at distances larger than 50m from the explosion, which is considered as the threshold for indirect effects with respect to human health.
- As of the tests with compressed helium gas, the maximum overpressure levels are lower than 140 mbar, representing the threshold for the first lethal effects (Test 3 and 4).

- Concerning the tests with compressed hydrogen gas, the maximum overpressure levels for the Tests 7 and 8 are higher than 200 mbar, the threshold for significant lethal effects with respect to human health.

The analysis of the experimental data shows that a significant fraction of the mechanical energy contributes to the blast wave strength (70-95%), while *some fraction* of chemical energy has to be taken into account. The experimental results were compared with the universal correlation of [5] where all mechanical energy and 12% of chemical energy are considered. It is revealed that most of the data fall below the best-fit line of the correlation [5], showing that in spite of its slightly conservative character, the correlation is applicable in such situations.

The analysis of the fireball evolution, based on fast camera videos, reveal interesting features of the fireball behaviour: a "breathing" oscillatory motion, having period of 17-20 ms, follows the initial fast growing period. This behaviour was not observed experimentally in an open area, although CFD simulations performed by Ulster University in a tunnel predicted this physical feature.

Overall, the presented test results constitute a unique database for the understanding and validation of energy release models at the road tunnel scale.

Acknowledgements

The authors are grateful to Clean Hydrogen Joint Undertaking for funding this research through grant agreement No 826193. The Joint Undertaking receives support from the European Union's Horizon 2020 research and innovation programme.

References

[1] N. Zalosh and R. Wayandt, "Hydrogen Fuel Tank Fire Exposure Burst Test," *SAE Paper Number 2005-01-1886,* 2005.

[2] C. Shen, L. Ma, G. Huang, Y. Wu, J. Zheng, Y. Liu and J. Hu, «Consequence assessment of high-pressure hydrogen storage tank rupture during fire test,» *Journal of Loss Prevention in the Process Industries,* vol. 55, pp. 223-231, 2018.

[3] M. Silvestrini , B. Genova and F. Leon Trujillo, «Energy concentration factor. A simple concept for the prediction of blast propagation in partially confined geometries.,» *Journal of Loss Prevention in Process Industries,* vol. 22, pp. 449-454, 2009.

[4] V. Molkov and S. Kashkarov, «Blast wave from a high-pressure gas tank rupture in a fire: Stand-alone and under-vehicle hydrogen tanks,» *International Journal of Hydrogen Energy,* pp. 12581-12603, 2015.

[5] V. Molkov and W. Dery, «The blast wave decay correlation for hydrogen tank,» *International Journal o f Hydrogen Energy,* pp. 31289-31302, 2020.

[6] D. Bouix, F. Sauzedde, P. Manicardi, M. Martin , D. Forero, E. Studer, G. Bernard-Michel, S. Koudriakov and H. Gueguen, «Full-scale tunnel experiments for fuel cell hydrogen vehicles: jet fire and tank explosion.,» *International COnference on Hydrogen Safety*, Edinburg, 2021.

[7] L. Heudier, «Formalisation du savoir et des outils dans le domaine des risques majeurs (EAT-DRA-76),» Rapport d'étude N°DRA-12-125630-04945B, 2013.

[8] W. Baker, P. Cox, P. Westine, J. Kulesz and R. Strehlow, Explosion hazards and evaluation, ELSEVIER, 1983.

[9] H. Liepmann and A. Roshko, Elements of Gasdynamics, Dover Publications, INC., 1956.

[10] M. Radulescu, «Compressible flow in a Noble-Abel stiffened gas fluid,» *Physics of Fluids,* vol. 32, p. 056101, 2020.

[11] V. Shentsov, «Effect of blast wave after tank rupture in a fire on a tunnel structure: CFD part,» *Digital stakeholders' workshop. HyTunnel-CS progect*, 2020.

[12] D. Makarov, V. Shentsov, M. Kuznetsov and V. Molkov, «Hydrogen Tank Rupture in Fire in the Open Atmosphere: Hazard Distance Defined by Fireball,» *Hydrogen,* vol. 2, pp. 134-146, 2021.